



Research article

Detailed mechanistic studies on PNN-palladium pincer complex catalyzed Suzuki-Miyaura cross-coupling reaction proceeding through a Pd^{II}/Pd^{III}/Pd^{IV} catalytic cycle

Gazal Sabharwal^a, Khilesh C. Dwivedi^a, Chandan Das^b, Thakur Rochak Kumar Rana^c, Arnab Dutta^{b,*}, Gopalan Rajaraman^{c,*}, Maravanji S. Balakrishna^{a,*}

^a Phosphorus Laboratory, Chemistry Department, Indian Institute of Technology Bombay, Powai, Mumbai 400076, India

^b Interdisciplinary Program of Climate Studies, Chemistry Department, Indian Institute of Technology Bombay, Powai, Maharashtra 400076, India

^c Department of Chemistry, Indian Institute of Technology Bombay, Powai, Maharashtra 400076, India



ARTICLE INFO

Keywords:

Palladium pincer

Phosphine

Suzuki-Miyaura cross coupling

Spectrochemical studies

Density functional theory

ABSTRACT

In this paper, synthesis, Pd and Pt complexes and catalytic investigations of a tridentate pincer ligand 2-(diphenylphosphanyl)-N-(pyridine-2-ylmethyl)benzamide, {(o-PPh₂)C₆H₄C(O)N(H)CH₂(C₆H₅N)} (1), (hereafter referred to as “PN(H)N” and its anionic form as “PNN”) is described. Reaction of 1 with MCl₂(COD) resulted in pincer complexes [MCl(PNN-κ³-P,N,N)] (Pd 2, Pt 3), whereas the same reaction with Pd(OAc)₂ afforded [CH₃C(O)OPd(PNN-κ³-P,N,N)] (4). The structures of all of the compounds are confirmed by single-crystal X-ray analysis. The palladium complex 4 promoted the Suzuki-Miyaura cross-coupling reaction between aryl halides and boronic acids to form the corresponding biphenyls in excellent yields. The catalytic investigation supported by spectroscopic studies and DFT calculations suggested the involvement of Pd^{II}/Pd^{IV} catalytic cycle via a short lived Pd^{III} intermediate, which transforms into Pd^{IV} species rapidly. The catalytic process proceeded with a very low catalyst loading under relatively mild reaction conditions.

1. Introduction

Phosphines with linkers capable of forming pincer complexes, are among the most widely used ligand systems in coordination chemistry and homogeneous catalysis, because of their ability to anchor the metal centre and facilitate redox processes and also metal-mediated organic transformations [1–4]. Steric and electronic properties around the donor atoms directly influence the stability, catalytic activity and selectivity of a catalyst, and in this context, hybrid or asymmetric pincer ligands of the type PNN [5,6], PNP [7,8] or PCP [9] are preferred because of their varied σ-donor and π-acceptor properties. Further, pincer complexes have a significant advantage in organic synthesis due to the following facts: i) their resistance to air and moisture, ii) robust tridentate meridional coordination, iii) often metal–ligand cooperation, and iv) thermal stability [10,11].

Carbon–carbon cross coupling reactions [12] catalyzed by Pd⁰ species or Pd⁰ *in situ* generated from Pd^{II} using a base are well-known [13–15] and the Pd⁰/Pd^{II}-driven catalytic mechanisms are also well studied [16]. In contrast, Pd^{II}/Pd^{IV}-catalytic cycles [17–19] received

little attention to date. No conclusive evidence of the presence of Pd^{III} or Pd^{IV} intermediates are shown in the mechanistic pathways, despite many claims regarding their possible role in catalysis [20–24]. Electroanalytical studies suggested the involvement of Pd^{II}/Pd^{IV} catalytic cycle via a Pd^{III} intermediate in certain reactions [25]. Hence, the complete story behind the chemically catalyzed Pd^{II}/Pd^{IV} cycles via Pd^{III} intermediate is yet to be unveiled.

A number of chemical oxidants including hypervalent iodine reagents [26], elemental halogens [27], electrophilic fluorination reagents [28], alkyl/aryl halides [29,30], ferrocenium salts, peroxides/O₂ [31], sulfonyl chlorides, and others have enabled the preparation of high-valent palladium species [32]. Many Pd^{III} and Pd^{IV} complexes containing neutral ligands such as bipyridine, naphthalene and biphenyl have been both spectroscopically and structurally characterized [33–39]. In contrast, reports on Pd^{III} and Pd^{IV} complexes of phosphorus-based ligands are scarce in the literature [40,41]. Herein, we report in detail, the synthesis, Pd and Pt chemistry of a new PN(H)N ligand {(o-PPh₂)C₆H₄C(O)N(H)CH₂(C₆H₅N)}. Additionally, Pd^{II}-PNN complex-promoted Suzuki-Miyaura cross coupling reaction between aryl halides and

* Corresponding authors.

E-mail addresses: krishna@chem.iitb.ac.in, msb_krishna@iitb.ac.in (M.S. Balakrishna).

<https://doi.org/10.1016/j.jcat.2024.115825>

Received 8 August 2024; Received in revised form 24 October 2024; Accepted 25 October 2024

Available online 28 October 2024

0021-9517/© 2024 Elsevier Inc. All rights are reserved, including those for text and data mining, AI training, and similar technologies.

phenyl boronic acids is also demonstrated. The reaction proceeds via Pd^{II}/Pd^{IV} mechanism involving a Pd^{III} intermediate evinced by mass spectrometry, XPS and EPR spectroscopic data and also extensive DFT studies [42–45]. Apart from spectroscopic data, DFT calculations were also employed to examine electronic structure, bonding, reactivity, and NMR data to evaluate and verify various intermediates formed during the coupling reaction. Despite the large body of literature available on Pd⁰/Pd^{II} systems, studies based on Pd^{II}/Pd^{IV} catalysts are rare; understanding its mechanism can offer important insight into the design of futuristic catalysts.

2. Experimental section

2.1. General procedures

All reactions were carried out under an inert atmosphere of dry nitrogen by using standard Schlenk and vacuum line techniques. Solvents were dried by usual methods and distilled before use. The compounds [MCl₂(COD)] (M = Pd [46] or Pt [46]) were prepared according to the published procedures. Other reagents were obtained from commercial sources and used after purification.

2.2. Instrumentation

NMR spectra were recorded on Bruker FT spectrometers (Avance-400 or 500) MHz at ambient probe temperatures. ¹³C{¹H} and ³¹P{¹H} NMR spectra were acquired using a broad band decoupling method. The spectra were recorded in CDCl₃ solutions with TMS as an internal standard; chemical shifts of ¹H and ¹³C{¹H} NMR spectra are reported in ppm downfield from TMS. The chemical shifts of ³¹P{¹H} NMR spectra are referred to 85 % H₃PO₄ as an external standard. Positive values indicate downfield shifts. Mass spectra were recorded using Bruker Maxis Impact LC-q-TOF Mass Spectrometer. Infrared spectra were recorded on a PerkinElmer *Spectrum One* FT-IR Spectrometer (Model No. 73465) in KBr disk. GC–MS analyses were performed on an Agilent 7890A GC system with an FID detector using a J & amp; WDB-1 column (10 m, 0.1 mm ID). The microanalyses were performed using Elementar (Germany) Vario Micro Cube CHNS Analyzer. The melting points of all compounds were determined on a Veego melting point apparatus and are uncorrected.

XPS of the reaction mixture was recorded using X-ray photoelectron spectroscopy (XPS: Axis Supra model, SHIMADZU group). Small aliquots of the reaction mixture were collected at various time intervals during the reaction. These aliquots were rapidly frozen in liquid nitrogen, and the XPS spectra were subsequently recorded for analysis. The reaction mixture (20 μL) was drop-casted on carbon paper, dried and used as an XPS sample. The wide spectrum was collected with 10 acquisitions and the high-resolution spectra of Pd 3d, C 1s, O 1s, N 1s and F 1s were collected with 20 acquisitions. A similar sample preparation method was employed for recording the EPR spectra. The EPR measurements were made with a JEOL model FA200 X-band (9.5 GHz) electron spin resonance spectrometer. The g-values were obtained from the EPR spectrum.

Cyclic voltammetry (CV) experiments were carried out at room temperature using Metrohm Autolab PGSTAT 204 potentiostat. All measurements were carried out in toluene (1 mM) in the presence of tetrabutylammonium tetrafluoroborate (0.1 M) as the supporting electrolyte. A standard three electrode system under N₂/Ar atmosphere was used with 1 mm glassy carbon disc as a working electrode, Ag as a reference electrode connected by a vycor tip and a platinum wire as a counter electrode. UV–vis absorption spectra were recorded using V-770 Double Beam UV–Visible/NIR Spectrophotometer using 1 cm path length quartz cuvette.

2.3. Crystal structure determination of complexes 1–4 and C

Single crystals of all complexes were mounted on a Cryolooop with a

drop of paratone oil and positioned in the cold nitrogen stream on a Bruker D8 Venture diffractometer. The data collections were performed at 100 K to 150 K using Bruker D8 Venture diffractometer with a graphite monochromatic Mo Kα radiation source (λ = 0.71073 Å) with the ω-scan technique. The data were reduced using CrysAlisPro Red 171.41.64.93a software. The structures were solved using Olex2 1.5 [47] with the ShelXT [48] structure solution program using intrinsic phasing and refined with SHELXL [49] refinement package using least-squares minimization. All non-hydrogen atoms were refined anisotropically. Hydrogen atoms were placed in calculated positions and included as riding contributions with isotropic displacement parameters tied to those of the attached non-hydrogen atoms. The given chemical formula and other crystal data do not consider the unknown solvent molecule(s). The reflections with error/esd more than 10 were excluded to avoid problems related to better refinement of the data. The data completeness is more than 99.8 % in most of the cases, which is enough to guarantee a very good refinement of data. The details of X-ray structural determinations are given in Table S5. Crystallographic data for the structures reported in this paper have been deposited with the Cambridge Crystallographic Data Centre as supplementary publication no. 2359369, 2359371-2359373 and 2359376 for compound 1, 2–4 and intermediate C respectively.

2.4. Computational details

In this investigation, we utilized Gaussian 16 (Gaussian, Inc., Wallingford, CT, 2016) for all DFT calculations. Grimme's dispersion-corrected B3LYP functional (B3LYP-D3) was employed for geometry optimization [50,51]. Geometry optimization and computation of imaginary frequencies were performed for all entities, encompassing reactants, intermediates, and transition states. The LanL2DZ basis set for Pd metal [52] and the 6-31G* basis set for C, H, N, O, and P, Cl [50,51,53,54] were used in the calculations. Solvation energy was incorporated into the gas phase energy using a more advanced level of theory (B3LYP-D3/def2-TZVP) [55]. Solvation energy determination employed the polarizable continuum model (PCM) with toluene as the solvent [56] accounting for electrostatic, dispersion-repulsion, and cavitation terms. Frequency calculations were conducted to identify minima on the potential-energy surface (PES) and final free energies were calculated by adding zero-point energy correction. Visualization of optimized geometries was done using Chemcraft 1.6 and Gaussview 6.0 (GaussView; SemicheM Inc, 2016). Gaussian 16 software was used for NBO (Natural Bond Orbital) [57,58] and WBI (Wiberg Bond Index) analyses [59] using DFT methods. NBO analysis provided detailed insights into bonding orbitals and natural charge distribution (see Table S3–S4), while WBI analysis offered bond index values indicating bond nature. All optimized geometries have been provided in Figure S92. Ab-initio calculations for EPR were carried out using the ORCA5.0.4 [60–63] software package using the B3LYP-G/TZVP(Pd atom), def2-SVP (remaining all atoms) setup in toluene using a conductor-like polarizable continuum model (CPCM) for solvation along the resolution of the identity (RI-JK) approximation [64]. D3BJ used for dispersion correction by the newer recommended Becke-Johnson damping (D3BJ). The relativistic effect was considered using the Dohgllass–Kroll–Hess (DKH) Hamiltonian [65]. The coordinates of all the optimized geometries are included in the Supporting Information.

2.5. Complexes preparation and characterization

2.5.1. Synthesis of {(o-PPh₂)C₆H₄C(O)N(H)CH₂(C₆H₅N)} (1)

To a thick-walled seal tube containing a magnetic stir bar were added 2-bromo-N-(pyridin-2-ylmethyl)benzamide (1. g, 3.434 mmol), Pd(PPh₃)₄ (0.238 g, 0.206 mmol, 6 mol%), K₂CO₃ (0.522 g, 3.774 mmol, 1.1 equiv), toluene (10 mL), and HPPH₂ (0.831 g, 4.464 mmol, 1.3 equiv). The tube was sealed and heated to 150 °C for 24 h with vigorous stirring. After 24 h, the reaction mixture was cooled, diluted with

dichloromethane (40 mL), and washed with distilled water (3 × 30 mL). The organic layer was dried over anhydrous Na₂SO₄ and filtered, and the solution was concentrated under vacuo to give **1** as a white colour solid, which was purified by flash chromatography over silica, eluting with 1:1 ethyl acetate/petroleum ether. Single crystals suitable for X-ray analysis were obtained by slow diffusion of petroleum ether into the dichloromethane solution of **1**. The monophosphine **1** was characterized by multinuclear NMR spectroscopy, mass spectrometry and by X-ray crystallography. Yield 70 % (0.950 g). **Mp**: 136–138 °C. ¹H NMR (400 MHz, CDCl₃) δ 8.47 (s, 1H), 7.75–7.68 (m, 2H), 7.39 (td, *J* = 7.5, 1.4 Hz, 2H), 7.36–7.17 (m, 13H), 6.97 (ddd, *J* = 7.6, 4.0, 1.3 Hz, 1H), 4.65 (d, *J* = 5.1 Hz, 2H). ³¹P{¹H} NMR (162 MHz, CDCl₃) δ –9.3. ¹³C{¹H} NMR (101 MHz, CDCl₃) δ 169.1, 156.2, 149, 141.3, 136.8, 134.3, 134.1, 133.9, 132.1, 130.3, 128.8, 128.6, 128.6, 127.8, 122.4, 122.3, 45. **HRMS(ESI)**, *m/z*: Calcd for C₂₅H₂₁N₂P₁O₁Na [M+Na]⁺: 419.1284; Found: 419.1284. **Anal. Calcd** for C₂₅H₂₁N₂O: C, 75.74; H, 5.34; N, 7.07. Found: C, 75.58; H, 5.39; N, 6.74. **FT-IR** (KBr disk, cm⁻¹): 3323 s (ν_{NH}), 3056 m, 1634 s (ν_{CO}), 1532 m, 1431 w, 1306 m, 1164 w, 1095 w, 746 s, 702 w.

2.5.2. Synthesis of [PdCl(PNN-κ³-P,N,N)] (**2**)

A solution of [PdCl₂(COD)] (0.036 g, 0.1261 mmol) in dichloromethane (10 mL) was added dropwise to a solution of **1** (0.05 g, 0.1261 mmol) also in dichloromethane (5 mL), and the mixture was stirred for 6 h and dried under vacuo to give a pale-yellow residue of **2**. The residue was washed with petroleum ether (1 × 10 mL) and dried to get an analytically pure product of **2** as a yellow solid. Single crystals of **2** suitable for X-ray analysis were obtained by slow diffusion of petroleum ether into the dichloromethane solution of **2**. Yield: 81 % (0.054 g). **Mp**: 154–156 °C. ¹H NMR (400 MHz, CDCl₃) δ 9.02 (q, *J* = 2.9 Hz, 1H), 8.60 (ddd, *J* = 8.1, 4.2, 1.4 Hz, 2H), 7.85 (td, *J* = 7.7, 1.7 Hz, 2H), 7.65–7.60 (m, 7H), 7.47–7.44 (m, 4H), 7.36–7.34 (m, 1H), 6.88 (ddd, *J* = 11.7, 7.8, 1.4 Hz, 1H), 5.23 (s, 2H). ³¹P{¹H} NMR (162 MHz, CDCl₃) δ 26.2. ¹³C{¹H} NMR (101 MHz, CDCl₃) δ 162.6, 147.4, 138.8, 133.9, 133.8, 132.5, 131.9, 131.8, 131.8, 131.4, 131.3, 128.6, 128.5, 128.3, 128.2, 120.3, 61.1. **HRMS(ESI)**, *m/z*: Calcd for C₂₅H₂₁N₂P₁O₁Cl₁Pd₁ [M+H]⁺: 537.0107 Found: 539.0107. **Anal. Calcd** for C₂₅H₂₀N₂OClPd: C, 55.88; H, 3.75; N, 5.21. Found: C, 55.89; H, 3.79; N, 5.23. **FT-IR** (KBr disk, cm⁻¹): 3057 w, 1580 s (ν_{CO}), 1542 s, 1437 m, 1374 s.

2.5.3. Synthesis of [PtCl(PNN-κ³-P,N,N)] (**3**)

A solution of [PtCl₂(COD)] (0.047 g, 0.1261 mmol) in dichloromethane (10 mL) was added dropwise to a solution of **1** (0.05 g, 0.1261 mmol) also in dichloromethane (5 mL), and the mixture was stirred for 6 h and dried under vacuo. The residue obtained was washed with petroleum ether (1 × 10 mL) and dried under vacuo to give compound **3** as a white solid. Single-crystals suitable for X-ray analysis were grown from a 1:1 mixture of dichloromethane and petroleum ether at 25 °C. Yield: 83 % (0.066 g). **Mp**: 235–238 °C. ¹H NMR (400 MHz, CDCl₃) δ 9.02 (q, *J* = 2.9 Hz, 1H), 8.60 (ddd, *J* = 8.1, 4.2, 1.4 Hz, 2H), 7.85 (td, *J* = 7.7, 1.7 Hz, 2H), 7.65–7.60 (m, 7H), 7.47–7.44 (m, 4H), 7.36–7.34 (m, 1H), 6.88 (ddd, *J* = 11.7, 7.8, 1.4 Hz, 1H), 5.23 (s, 2H). ³¹P{¹H} NMR (162 MHz, CDCl₃) δ, –0.2 ¹J_{PTIP} = 3583 Hz. ¹³C{¹H} NMR (101 MHz, CDCl₃) δ 147.4, 138.8, 133.9, 133.8, 132.5, 131.9, 131.8, 131.8, 131.4, 131.3, 128.6, 128.5, 128.3, 128.2, 120.3, 61.1. **HRMS(ESI)**, *m/z*: Calcd for C₂₅H₂₁N₂P₁O₁Cl₁Pt₁ [M+H]⁺: 626.0722 Found: 627.0717. **Anal. Calcd** for C₂₅H₂₀N₂OClPt: C, 47.97; H, 3.22; N, 4.48. Found: C, 47.58; H, 3.30; N, 4.50. **FT-IR** (KBr disk, cm⁻¹): 3056 w, 1542 s (ν_{CO}), 1434 s, 1379 s.

2.5.4. Synthesis of [CH₃C(O)OPd(PNN-κ³-P,N,N)] (**4**)

A solution of Pd(OAc)₂ (0.028 g, 0.1261 mmol) in dichloromethane (10 mL) was added dropwise to a solution of **1** (0.05 g, 0.1261 mmol) also in dichloromethane (5 mL), and the mixture was stirred for 6 h and dried under vacuo to give a pale yellow residue of **4**. The residue was washed with petroleum ether (1 × 10 mL) and dried to get an analytically pure product of **4** as a yellow solid. Single crystals of **4** suitable for

X-ray analysis were obtained by slow diffusion of petroleum ether into the dichloromethane solution of **4**. Yield: 80 % (0.023 g). **Mp**: 183–185 °C. ¹H NMR (400 MHz, CDCl₃) δ 8.47–8.44 (m, 1H), 8.35–8.31 (m, 1H), 7.86–7.82 (m, 1H), 7.78–7.72 (m, 4H), 7.60–7.57 (m, 1H), 7.52 (d, *J* = 2.4 Hz, 1H), 7.47–7.43 (m, 5H), 7.36–7.29 (m, 3H), 6.97–6.92 (m, 1H), 5.15 (s, 2H), 1.54 (s, 3H). ³¹P{¹H} NMR (202 MHz, CDCl₃) δ 24. ¹³C{¹H} NMR (101 MHz, CDCl₃) δ 177.1, 166.4, 162.5, 146.9, 139.2, 134.4, 134.3, 131.6, 131.6, 128.9, 128.8, 127.3, 126.7, 122.7, 122.6, 120.9, 60.1, 22.7. **HRMS(ESI)**, *m/z*: Calcd for C₂₇H₂₃N₂P₁O₃Pd₁Na [M+Na]⁺: 583.0373; Found: 583.0383. **Anal. Calcd** for C₂₇H₂₃N₂O₃PPd: C, 57.82; H, 4.13; N, 4.99. Found: C, 57.68; H, 4.078; N, 5.01. **FT-IR** (KBr disk, cm⁻¹): 3048 w, 2828 w, 1627 s (ν_{CO}), 1540 s (ν_{CO}), 1436 m, 1369 s, 1319 s, 1104 m.

2.5.5. Synthesis of [Pd(PNN-κ³-P,N,N)] (**C**)

The catalytic reaction involving iodobenzene and phenyl boronic acid was halted at various time intervals, and small aliquots of the reaction mixture were extracted and subsequently frozen to promote crystallization for the isolation of intermediates. Crystals of complex **C**, were successfully obtained from the reaction vial that had been frozen after 10 h of reaction. ¹H NMR (500 MHz, CDCl₃) δ 9.04 (ddd, *J* = 5.5, 3.6, 1.5 Hz, 1H), 8.63 (ddd, *J* = 8.1, 4.2, 1.3 Hz, 1H), 7.87 (td, *J* = 7.7, 1.6 Hz, 1H), 7.69–7.62 (m, 5H), 7.58–7.53 (m, 3H), 7.47 (ddd, *J* = 8.6, 6.9, 2.8 Hz, 4H), 7.40–7.34 (m, 2H), 6.91 (ddd, *J* = 11.7, 7.7, 1.3 Hz, 1H), 5.26 (s, 2H). ¹³C{¹H} NMR (126 MHz, CDCl₃) δ 162.8, 147.5, 143, 138.9, 133.9, 133.8, 132.6, 131.8, 131.8, 131.4, 128.7, 128.6, 122.4, 122.4, 120.4, 120.4, 61.2. ³¹P{¹H} NMR (162 MHz, CDCl₃) δ 29.5. **HRMS(ESI)**, *m/z*: Calcd for C₂₅H₂₁N₂P₁O₁I₁Pd₁ [M+H]⁺: 628.9466 Found: 628.9472. **FT-IR** (KBr disk, cm⁻¹): 3061 w, 1586 s (ν_{CO}), 1532 s, 1373 s.

2.6. General procedure for the Suzuki-Miyaura cross coupling reaction

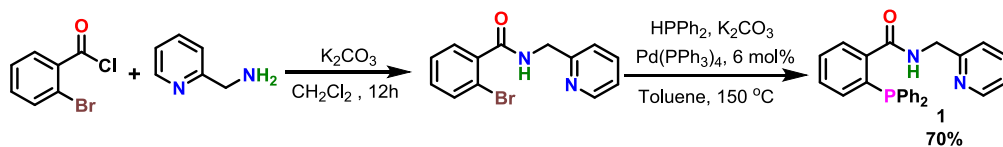
The reactions were performed in a closed vessel containing a mixture of substituted aryl chloride/bromide (1.0 equiv.), phenyl boronic acid (1.5 equiv.), base (2.0 equiv.) and palladium catalyst **4** (0.5 mol%), in toluene (2 mL). The reaction mixture was heated to 110 °C for 18 h. The residual mixture was diluted with H₂O (10 mL) and extracted twice with ethyl acetate (10 mL). The combined organic fractions were dried over Na₂SO₄, and the solvent was evaporated under reduced pressure to give a crude product. The crude product was purified by silica gel column chromatography using petroleum ether/ethyl acetate as eluent.

3. Results and discussion

3.1. Synthesis of 2-(diphenylphosphanyl)-N-(pyridine-2-ylmethyl) benzamide (**1**)

The reaction of pyridin-2-ylmethanamine with 2-bromobenzoyl chloride in 1:1 M ratio afforded amide derivative, which on further treatment with diphenylphosphine in the presence of catalytic amount of Pd(PPh₃)₄ and K₂CO₃ afforded PN(H)N ligand **1** in 70 % yield [66] (Scheme 1). The ³¹P{¹H} NMR spectrum of **1** showed a single resonance at –9.4 ppm. In ¹H NMR spectrum, the NH proton appeared as a triplet centered at 7.17 ppm with a ²J_{HH} coupling of 4 Hz due to adjacent methylene protons, which was further confirmed by ¹H–¹H COSY spectrum (Fig. S4). The ¹³C{¹H} NMR spectrum of **1** showed carbonyl carbon resonance at 169 ppm. The IR spectrum of **1** showed the secondary amide band at 3323 cm⁻¹, whereas the ν_{CO} appeared at 1634 cm⁻¹.

Ligand **1** was crystallized in dichloromethane and its molecular structure was established by single crystal X-ray analysis. The perspective view of **1** is shown in Fig. 1, and the specified bond lengths (Å) and bond angles (°) are given in the figure caption.



Scheme 1. Synthesis of PN(H)N ligand 1.

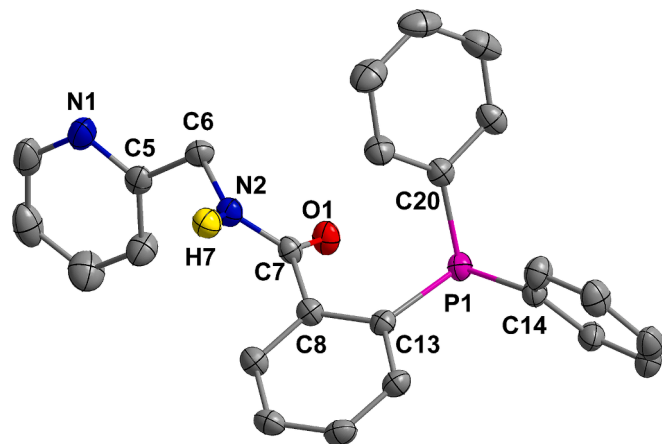


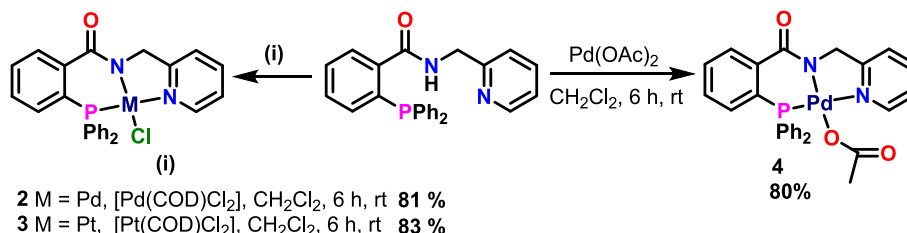
Fig. 1. Single X-ray crystal structure of ligand 1. All hydrogen atoms have been omitted (except H7) for clarity. Displacement ellipsoids are drawn at 50% probability level. Selected bond lengths [Å] and bond angles [°]: O1-C7 1.2339 (18), N2-C7 1.3381(19), N2-H7 0.835(19), P1-C13 1.8453(15), N1-C5 1.341 (2), N2-C7-O1 123.44(14), C20-P1-C14 100.77(7), C13-P1-C14 101.62(7), C5-C6-N2 112.72(12).

3.2. Synthesis of Pd^{II} and Pt^{II} complexes 2–4

Pincer complexes of palladium and platinum, [MCl{(PNN)-κ³-P,N,N}] (2 Pd, 3 Pt) were prepared by reacting PN(H)N (1) with [MCl₂(COD)] in CH₂Cl₂ at room temperature (Scheme 2). Reaction of 1 with [Pd(OAc)₂] in CH₂Cl₂ resulted in [Pd(κ¹-OC(O)CH₃){(PNN)-κ³-P,N,N}] (4). The disappearance of NH proton in the ¹H NMR spectra of complexes 2–4, confirmed the pincer complex formation. The ³¹P{¹H} NMR spectra consist of singlets at 26.2 and –0.2 ppm, respectively, for 2 and 3, with platinum complex 3 showing a ¹J_{P-Pt} value of 3583 Hz; a singlet was observed at 24 ppm for complex 4. The IR spectrum of 4 showed two distinct C–O stretching bands (ν_{CO}) at 1627 and 1540 cm^{–1}, respectively, for acetate and the ligand carbonyl groups.

The molecular structures of 2–4 were confirmed by single crystal X-ray analysis. All the pincer complexes are crystallized by slow diffusion of petroleum ether into the dichloromethane solution of the corresponding complexes. The molecular structures of 2–4 are shown in Fig. 2, whereas the selected bond lengths and bond angles are listed in Table 1.

The metal centres in complexes 2–4 are in a distorted square planar environment. The maximum distortion from linearity around the metal center can be seen in case of 4, where the P1–Pd–N1 bond angle is 171.47

Scheme 2. Syntheses of Pd^{II} and Pt^{II} complexes 2–4.

(7)^o.

3.3. Catalytic studies

3.3.1. Suzuki-Miyaura cross coupling reaction between aryl halides and boronic acids catalyzed by palladium complex 4

The most essential routes to make C–C and C–N bonds to generate building materials for polymers, chemical and pharmaceutical industries are cross coupling reactions[67]. Palladium complex catalyzed Suzuki-Miyaura reaction is one of the most widely recognized cross coupling reactions because of the functional group tolerance for a variety of substrates[68–73]. Although Pd is expensive, Pd-catalysts are less toxic and are resistant to moisture and oxygen as opposed to many other metal catalysts[74–77].

Palladium complex 4 catalyzed the Suzuki-Miyaura cross coupling reaction with product formation in 80–99 % yield. The optimized reaction conditions are mentioned in Table 2. The percentage yield of the biphenyl product was monitored via gas chromatography (GC) employing chlorobenzene and phenylboronic acid as model substrates, and the corresponding GC plots are provided in the Supporting Information. Initial evaluation of coupling between chlorobenzene and phenylboronic acid in the absence of the catalyst 4 did not show any conversion (entry 1). Upon the addition of 0.06 mol% of catalyst 21 % yield was observed (entry 2). With increase in catalyst loading, the yield increased steadily (entries 3–5). The same reaction with Pd(OAc)₂ (0.5 mol%) resulted in low yield (entry 17). Various bases such as K₃PO₄, KOH, NaOH, Cs₂CO₃, NaO^tBu and KO^tBu were scanned, among them K₃PO₄ showed better performance (entries 5–10). Among the solvents such as toluene, 1,4-dioxane, THF, ethanol, methanol and water, toluene was found to be efficient for the coupling process (entries 5 and 11–14). On increasing the reaction temperature to 130 °C, the yield decreased (entry 15). Similar trend was observed on lowering the temperature to 25 °C (rt) (entry 16). The yield decreased on increasing and decreasing the reaction time (entries 18–19) with optimized time being 18 h. The reaction showed no product formation in the absence of base (entry 20). After optimizing the reaction conditions with Cat 4 (0.5 mol%), K₃PO₄ as the base and toluene as solvent at 110 °C for 18 h, the substrate scope was examined as depicted in Table 3. To avoid any ambiguity regarding homo-coupled products, the reaction conditions were optimized using 4-methylchlorobenzene instead of chlorobenzene, along with phenylboronic acid as model substrates, and monitored using GC–MS. The optimization data are presented in Table S1, and the corresponding GC–MS plots are included in the Supporting Information. It was observed that extending the reaction time beyond 18 h led to the homo-coupled product due to the excess boronic acid used (1.5 equivalent) in the reaction (See Fig. S87). The same reaction of boronic acid with 4-

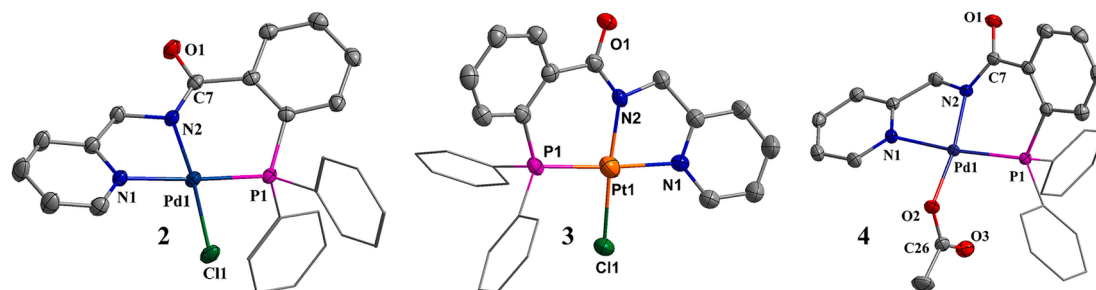


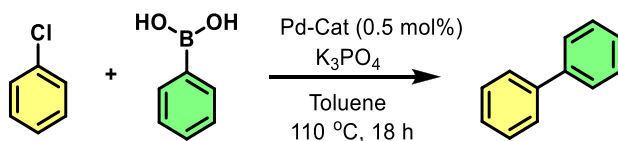
Fig. 2. Molecular structures of complexes 2–4. All hydrogen atoms and solvent molecules have been omitted for the sake of clarity. Displacement ellipsoids are drawn at 50 % probability level.

Table 1
Selected bond lengths (Å) and bond angles (°) of 2–4.

	2 (Pd)	3 (Pt)	4 (Pd)
N2-M	2.006(2)	1.999(2)	1.998(2)
P1-M	2.2114(8)	2.2052(9)	2.2086(7)
N1-M	2.089(2)	2.079(3)	2.066(2)
M-Cl	2.3065(8)	2.3224(8)	–
M-O2	–	–	2.029(2)
C7-O1	1.247(3)	1.249(4)	1.240(3)
N2-C7	1.333(3)	1.329(4)	1.341(4)
P1-M-N1	174.88(6)	176.31(7)	171.47(7)
P1-M-Cl1	90.63(2)	90.87(3)	–
P1-M-O2	–	–	97.11(6)
N1-M-Cl1	94.09(6)	92.81(8)	–
N1-M-O2	–	–	91.36(9)
N2-M-Cl1	174.91(6)	173.14(7)	–
N2-M-O2	–	–	171.97(8)
P1-M-N2	93.43(6)	94.68(7)	89.64(7)
N1-M-N2	81.75(9)	81.63(10)	82.00(9)

methyl chlorobenzene in 1:1 M ratio yielded the desired product 4-methyl-1,1'-biphenyl in 98 % yield and no homo-coupled product was formed even upon increasing the reaction time (Fig. S88).

Based on the ideal reaction conditions, coupling reactions between several aryl chlorides/bromides and phenylboronic acids were carried out to assess the overall effectiveness of the catalytic system. Excellent yields were achieved with both the electron rich and electron deficient aryl chlorides/bromides. Different derivatives of boronic acids coupled effectively to produce the corresponding biphenyl in 80–99 % yields. These findings are comparable to or better than those reported with other catalytic systems [78–80].



3.3.2. Mechanistic insights from DFT calculations

DFT calculations were carried out using the Gaussian16.C suite of program [81] employing B3LYP-D3/def2-TZVP (PCM) // B3LYP-D3/LanL2DZ(Pd); 6-31G*(rest atoms) level of theory at 298.13 K temperature (see computational details) [42–45]. The schematic mechanism adapted based on the experimental evidences gathered in this work and from earlier literature precedents, is depicted in Scheme 3 [82–91]. The DFT calculations were initiated to understand the

Table 2
Optimization of the reaction condition for Suzuki-Miyaura cross coupling reaction^a.

Entry	Catalyst [mol%]	Base	Solvent	Yield [%]
1	No Cat	K ₃ PO ₄	Toluene	0
2	0.06	K ₃ PO ₄	Toluene	21
3	0.125	K ₃ PO ₄	Toluene	42
4	0.25	K ₃ PO ₄	Toluene	73
5	0.5	K ₃ PO ₄	Toluene	99
6	0.5	KOH	Toluene	52
7	0.5	NaOH	Toluene	13
8	0.5	CS ₂ CO ₃	Toluene	82
9	0.5	NaO ^t Bu	Toluene	27
10	0.5	KO ^t Bu	Toluene	74
11	0.5	K ₃ PO ₄	1,4-dioxane	85
12	0.5	K ₃ PO ₄	THF	22
13	0.5	K ₃ PO ₄	EtOH	11
13	0.5	K ₃ PO ₄	MeOH	8
14	0.5	K ₃ PO ₄	H ₂ O	0
15 ^b	0.5	K ₃ PO ₄	Toluene	84
16 ^c	0.5	K ₃ PO ₄	Toluene	31
17 ^d	0.5	K ₃ PO ₄	Toluene	35
18 ^e	0.5	K ₃ PO ₄	Toluene	77
19 ^f	0.5	K ₃ PO ₄	Toluene	48
20	0.5	No Base	Toluene	0

^a Aryl chloride (0.50 mmol), phenyl boronic acid (0.75 mmol), K₃PO₄ (1 mmol) and solvent (2 mL), 110 °C, yield was determined by GC using chlorobenzene and phenylboronic acid as model substrates.

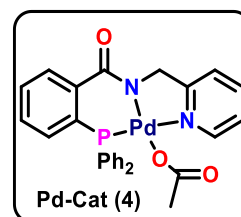
^b Temp, 130 °C.

^c Temp, rt.

^d Catalyst, Pd(OAc)₂.

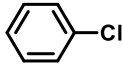
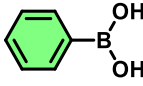
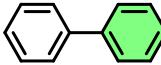
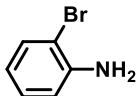
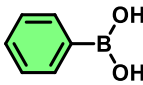
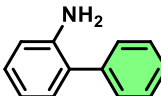
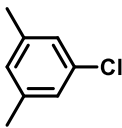
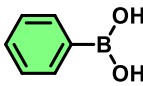
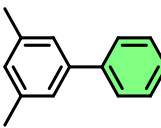
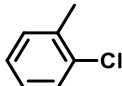
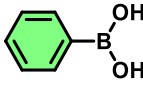
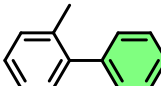
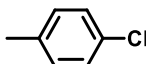
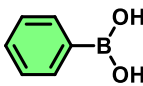
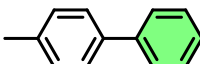
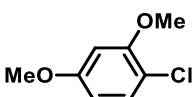
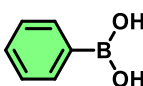
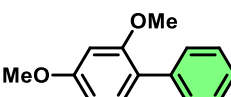
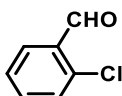
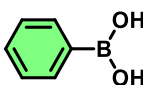
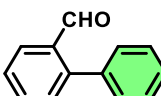
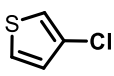
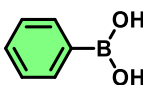
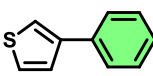
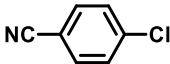
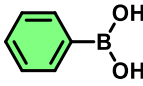
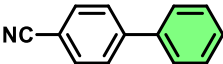
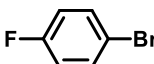
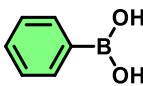
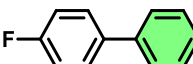
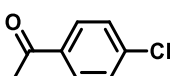
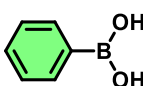
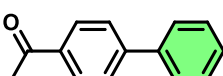
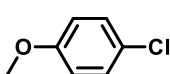
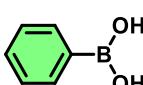
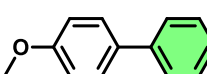
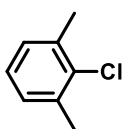
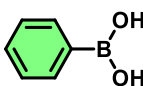
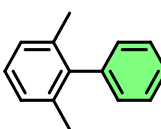
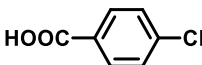
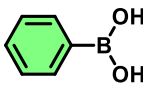

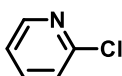
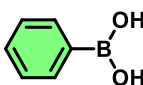
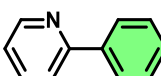
^e Reaction time, 16 h.

^f Reaction time, 24 h.



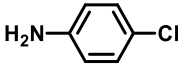
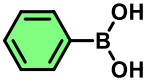
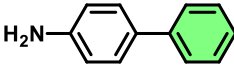
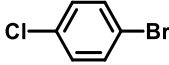
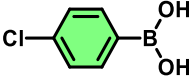
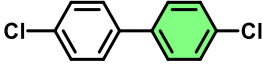
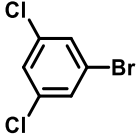
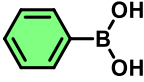
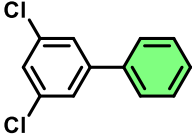
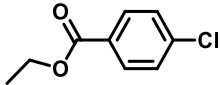
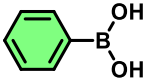
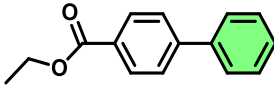
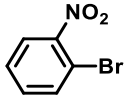
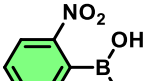
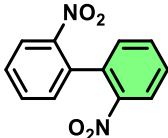
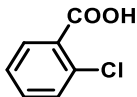
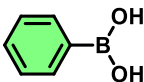
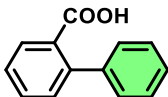
bonding nature of the complex 4; the frontier orbitals corresponding to the *d*-based orbitals of Pd along with its energy are shown in Fig. 3. The optimized geometry of 4 (Fig. 3), is consistent with the X-ray geometry (See Table S2 for comparison). The energy difference $\Delta(E_z^2 - E_{xy}^2)$ is estimated to be 3.29 eV with the square planar electronic configuration: $(d_{xz})^2 (d_{yz})^2 (d_{xy})^2 (d_z^2)^2 (d_{xy}^2)^0$ (Fig. 3). The d_z^2 orbital is significantly destabilized due to the interaction with *p*-orbital of the phosphorous ligand, which helps to reduce the energy for the

Table 3
Substrate scope for Suzuki-Miyaura cross coupling reaction.

Entry	ArX	Ar'B(OH) ₂	Product	% Yield
1				99
2				97
3				99
4				96
5				97
6				95
7				86
8				90
9				81
10				99
11				99
12				98
13				98
14				87
15				84

(continued on next page)

Table 3 (continued)

Entry	ArX	Ar'B(OH) ₂	Product	% Yield
16				92
17				81
18				83
19				99
20				80
21				97

Conditions: Aryl chloride/bromide (0.5 mmol), phenyl boronic acid (0.75 mmol), K₃PO₄ (1 mmol), toluene 2 mL, 110 °C, and catalyst (0.5 mol%). All are isolated yields.

oxidation process.

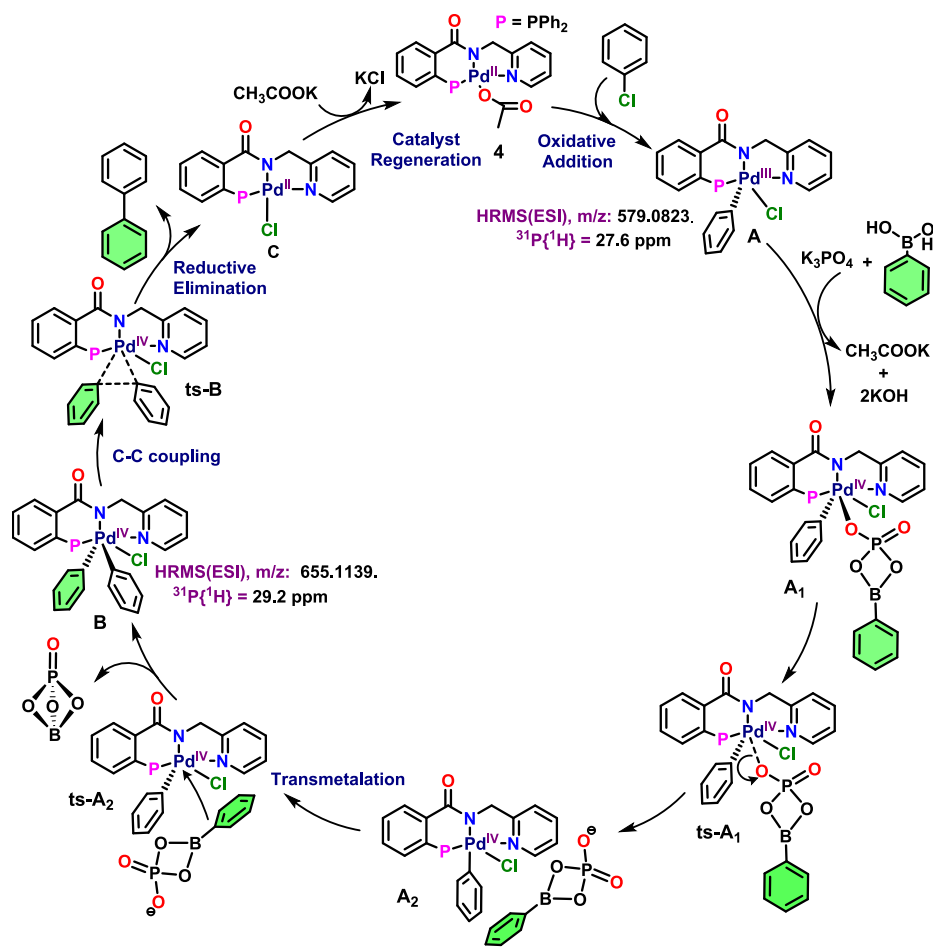
DFT calculations were initiated by considering complex **4** as an active catalyst, which undergoes oxidative addition with aryl chloride and forms a Pd^{III} intermediate **A** which is found to be endothermic by 92.1 kJ/mol. The ³¹P{¹H} NMR spectra of **A** showed a signal at 27.6 ppm and ESI-MS spectrum showed *m/z* 579.0823 for [M–Cl]⁺ ion. The XPS and EPR spectra further confirmed the formation of Pd^{III} species [35,92] (Fig. 6 and Fig. 7). The DFT optimised geometry of **A** as shown in Fig. 3, revealed that the unpaired electron located in the d_{z²} orbital with significant delocalisation to –Cl ligand. Further we have also computed the g-tensors from DFT calculations using ORCA suite software, which completely match the experimental g-values reported. An additional possibility of **A** being a six-coordinate species (**A'**) with acetate group in the sixth position was considered, not only the formation of such species is more endothermic, the computed g-tensors strongly deviate from the experiments ruling out the possibility of such a species (See Fig. S94).

In the next step, the phenyl boronic acid with potassium phosphate forms 4-phenyl-1,3,2,4-dioxaphosphaboretan-2-olate-2-oxide which coordinates to **A** to form intermediate **A**₁ which is more stable than **A** by –54.8 kJ/mol. With the cleavage of Pd–O bond, intermediate **A**₁ transforms into intermediate **A**₂ via transition state (**ts-A**₁) with an energy barrier of 124.2 kJ/mol. A relatively high kinetic energy barrier stems from very large distortions reflected in the estimated deformation energy (82.5 kJ/mol). Strong distortions in the geometry are also reflected in the estimated Root Mean Square Deviation (RMSD) between **ts-A**₁ from **A**₁ (1.1576). The intermediate **A**₂ undergoes transmetalation via Pd–C(phenyl) formation with an energy barrier of 74.9 kJ/mol and forms a highly stable intermediate **B** (–36.9 kJ/mol). In the next step, intermediate **A**₂ undergoes transmetalation via Pd–C(phenyl) formation with an energy barrier of 74.9 kJ/mol and forms a relatively stable intermediate **B** (–36.9 kJ/mol). Intermediate **B** was characterized by ³¹P{¹H} NMR and ESI-MS spectral data. The ³¹P{¹H} NMR spectrum of **B** showed a signal at 29.2 ppm and ESI-MS spectra of **B** showed molecular ion peak at *m/z* 655.1139 corresponding to [M–Cl]⁺ ion. The presence

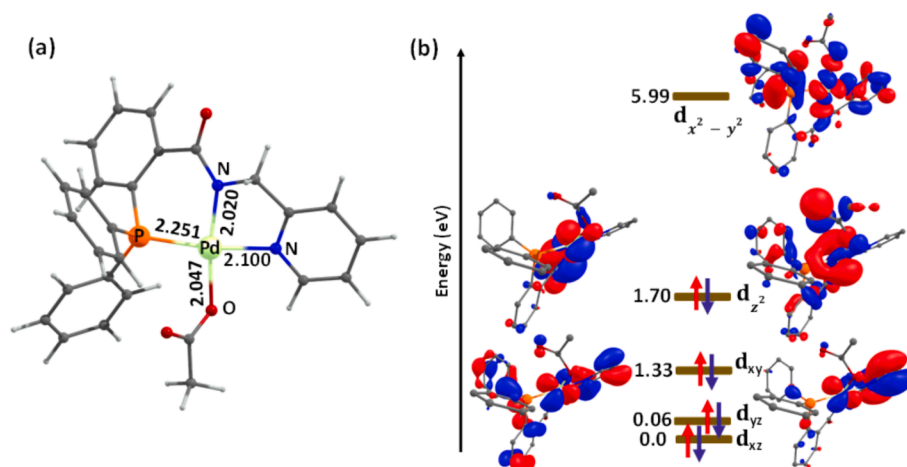
of Pd^{IV} in **B** was further confirmed by XPS spectra (Fig. 7) [26]. Although intermediate **B** is relatively stable species in the PES computed, given the fact that the temperature of the reaction is sufficiently high (110 °C), this species is expected to undergo C–C coupling in the next step, which leads to the reductive elimination of C–C coupled product via **ts-B** resulting in the formation of species **C**. The energy barrier for **ts-B** is 68.3 kJ/mol for C–C bond formation. The complex **C** (4.5 kJ/mol) reacts with potassium acetate to generate catalytic precursor **4**. Complex **C** has been isolated and structurally characterized. The computed potential energy profile diagram for coupling of aryl chloride and phenyl boronic acid in Suzuki-Miyaura coupling catalytic cycle with solvent phase free energies (ΔG in kJ/mol), is shown in Fig. 4.

In order to gain insight into the mechanism, the progress of the model reaction was monitored by variable-time ³¹P{¹H} NMR in a J. Young NMR tube in toluene. Initially a single peak corresponding to the complex **4** was observed at 24 ppm. After 4 h, the reaction mixture showed two peaks at 24 and 27.6 ppm, which indicates the partial conversion of Pd^{II} to Pd^{III} species via oxidative addition. After 8 h, the NMR spectrum showed a single peak at 27.6 ppm, indicating complete conversion to Pd^{III} species. After 10 h a single peak was observed at 29.2 ppm indicating the conversion of Pd^{III} to Pd^{IV} species via transmetalation. After 12 h, the spectrum showed two peaks at 23.9 and 29.1 ppm, respectively, for Pd^{II} and Pd^{IV}, as a result of reductive elimination. At the end of the reaction, i.e. after 18 h, a single peak observed at 24 (*ca* 23.9) ppm indicated the regeneration of the catalyst (Fig. 5). The ³¹P{¹H} NMR calculated values match closely with the experimental data as depicted in Table 4. The regeneration of the catalyst **4** from complex **C** was further confirmed by monitoring the reaction of complex **C** directly with potassium acetate with time dependent ³¹P{¹H} NMR spectroscopy (See Fig. S91).

To find out the reactive intermediates in the catalytic cycle, a series of Electron Paramagnetic Resonance (EPR) experiments were carried out at different time intervals. To investigate the role of base, EPR was recorded for the reaction mixture with and without base. We found a



Scheme 3. A plausible mechanism for the Suzuki-Miyaura cross coupling reaction.

Fig. 3. (a) Computed structural parameter of complex **4** and (b) the eigenvalue plot computed at B3LYP-D3 level of theory for d -orbitals for catalyst plotted using an iso-surface value of 0.035.

free radical signature (at $g \sim 2.00$) in the presence of a base, whereas in the absence of a base EPR signal was not observed. To check the oxidation state of Pd, EPR was recorded after 7 h that displayed a rhombic, anisotropic signal with $g_x = 2.27$, $g_y = 2.13$ and $g_z = 2.09$, characteristic of a Pd^{III}, d^7 centre with d_z^2 as ground state [92]. We have also computed the g -tensors for intermediate **A** from DFT calculations independently, which also supports rhombic anisotropy, albeit with a minor-variation between g_x and g_y values ($g_x = 2.153$, $g_y = 2.124$ and g_z

$= 2.011$). These minor variations are due to the DFT methods which do not yield accurate g -tensors compared to other methods such as ab initio CASSCF as suggested by us earlier [93]. Similarly, the EPR recorded after 10 h was identical to the spectra recorded after 7 h, albeit the intensity was reduced by $\sim 67\%$. This reduction in EPR signal signifies the conversion of Pd^{III} to Pd^{IV} (Fig. 6). Further, XPS performed after 7 h of the reaction, confirmed the formation of Pd^{III} intermediate. Similar XPS study conducted after 10 h, confirmed the formation of Pd^{IV} species [35]

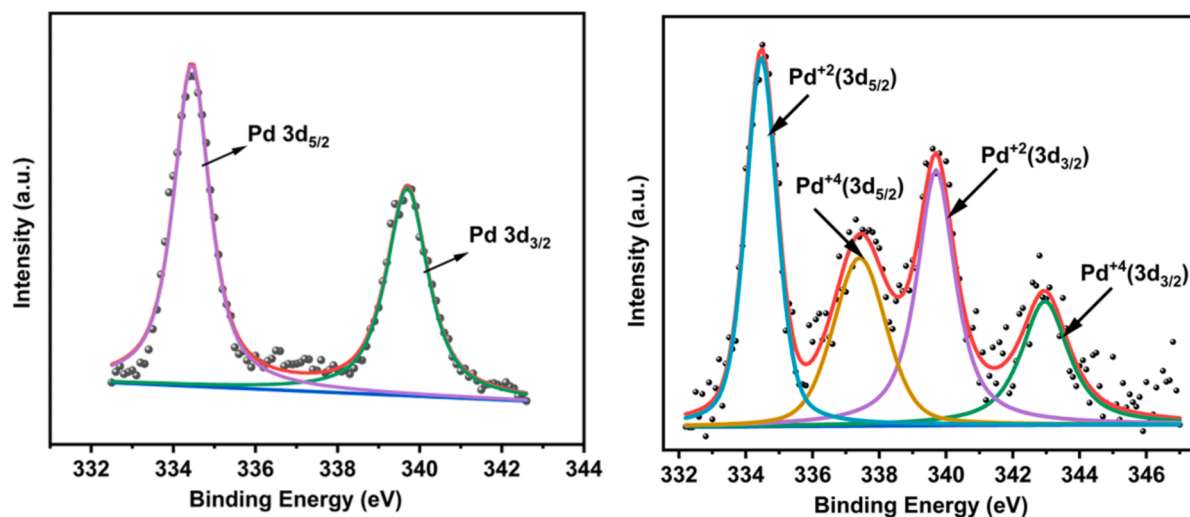


Fig. 7. XPS of the reaction mixture after 7 h and 10 h, showing the formation of Pd^{III} and Pd^{IV} species, respectively.

Table 4
³¹P{¹H} variable-time NMR data.

Species	Chemical Shift (Calc.)	Chemical Shift (Expt.)
4	23.8	24.0
A	26.4	27.6
B	28.4	29.2

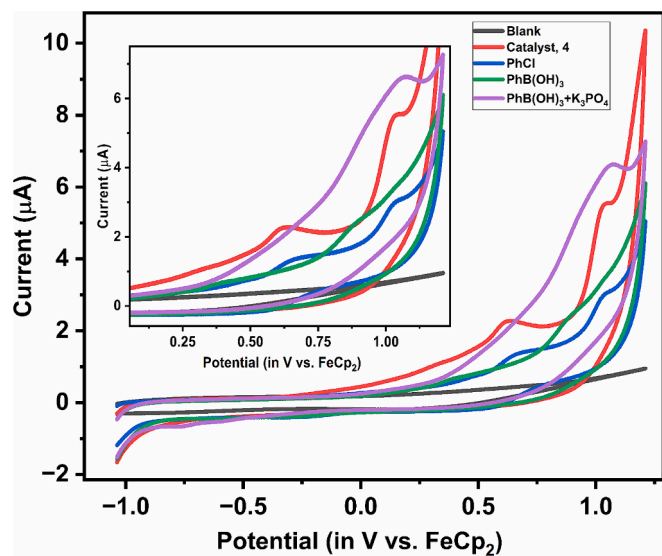


Fig. 8. Cyclic voltammogram (CV) of reactants (inset: enlarged CV diagram) Scan Rate: 0.1 V/s, Working Electrode: Glassy Carbon Disc (1 mm in diameter), Reference Electrode: Standard Ag/AgCl electrode (3 M KCl), Counter Electrode: Platinum wire. Supporting Electrolyte: tetra butyl ammonium tetrafluoroborate [NBu₄BF₄].

of reactants, not only the oxidation peaks were shifted, but also the oxidative current was increased, suggesting the importance of base for the reaction to drive the reaction forward via an active catalytic cycle.

3.3.3. Comparative study of aryl chloride versus aryl iodide for C–C coupling

To understand the mechanism and to quantitatively measure the rate of the Suzuki reaction, attempts were made to compare the reactivity of

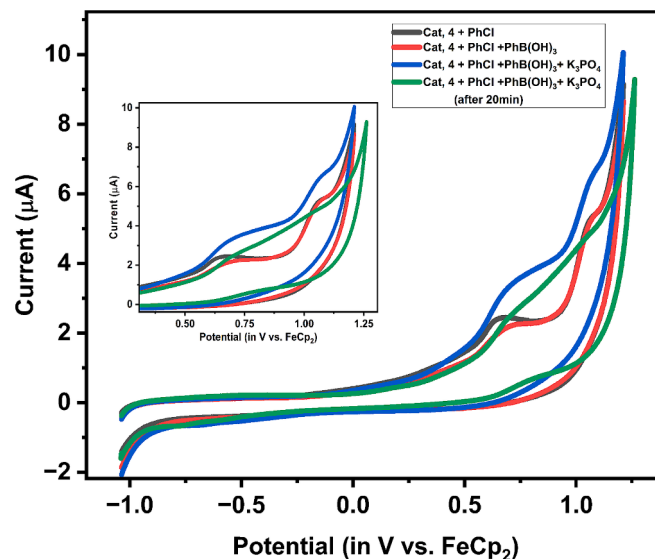


Fig. 9. Cyclic voltammogram (CV) plotted after the addition of reactants one by one (inset: enlarged CV diagram) Scan Rate: 0.1 V/s, Working Electrode: Glassy Carbon Disc (1 mm in diameter), Reference Electrode: Standard Ag/AgCl electrode (3 M KCl), Counter Electrode: Platinum wire. Supporting Electrolyte: tetrabutylammonium tetrafluoroborate [NBu₄BF₄].

aryl chloride versus aryl iodide. The complete reaction profile was modelled for aryl iodide and the potential energy comparison showed evidence of similar reactivity pattern in case of both aryl chloride and aryl iodide for C–C coupling reaction (Fig. 10). It has been observed that the reactivity pattern for aryl iodide has a lower energy barrier for **ts-A**₁ which represents the rate determining step for the reaction. Iodine, being a soft donor; donates more electron density to Pd^{IV}, which is also verified by natural charge on metal ion for **ts-A**₁. The intermediate **C** was also isolated and crystallized as a Pd-iodide pincer complex from the reaction mixture (Fig. 11).

To further probe the mechanism, UV–Visible spectra were plotted for the reaction mixture recorded at 90 °C for 5.5 h with chlorobenzene as the model substrate. The *in-situ* UV–visible analysis of the reaction mixture revealed the gradual decrease of an absorption band at 317 nm and shifting to 310 nm with time, signifying the conversion of Pd^{II} to Pd^{III} complex (Fig. 12-a) [25]. A shift in the absorption band from 286

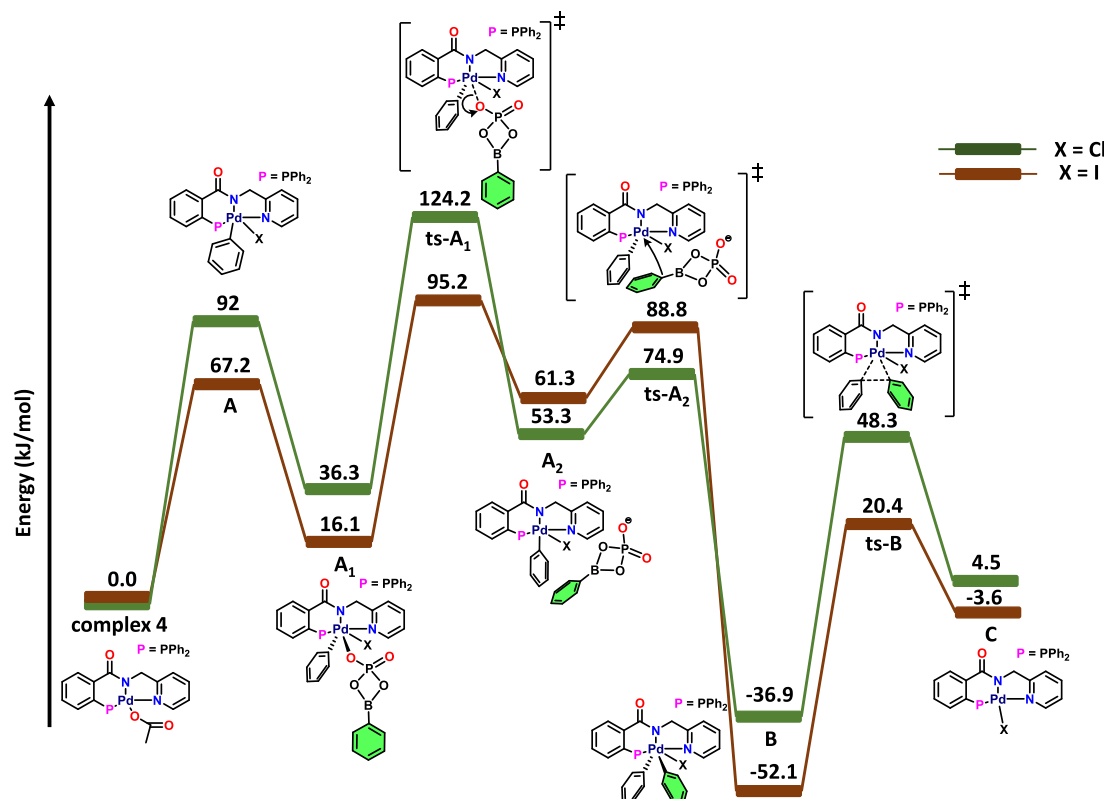


Fig. 10. Comparative study of iodide with chloride ligand to understand the feasibility of reaction with iodide ligand for Suzuki-Coupling catalytic cycle.

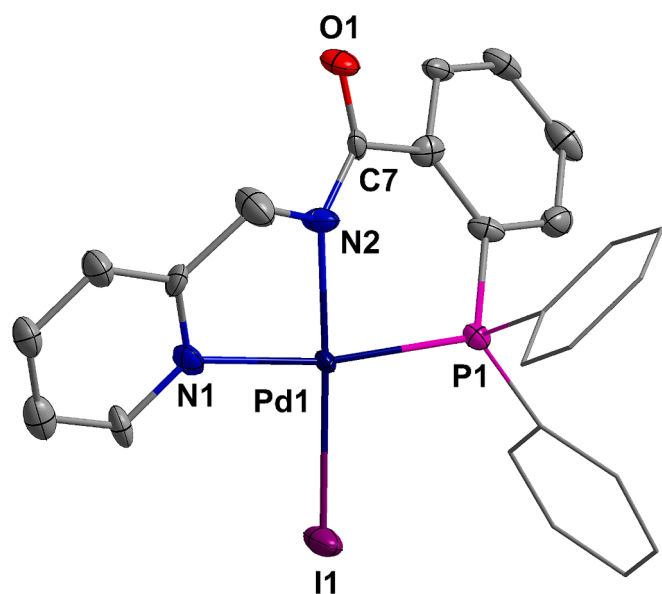


Fig. 11. Single X-ray crystal structure of complex C (in case of iodobenzene) All hydrogen atoms have been omitted for clarity. Displacement ellipsoids are drawn at 50% probability level. Selected bond lengths [Å] and bond angles [°]: Pd1-I1 2.5941(9), Pd1-P1 2.205(2), Pd1-N1 2.101(7), Pd1-N2 2.016(9), P1-Pd1-I1 96.61(6), N2-Pd1-I1 176.6(3), N1-Pd1-I1 96.1(2), N1-Pd1-P1 164.3(2).

nm to 276 nm with an increase in the intensity of the absorption band indicated more $\pi - \pi^*$ transition in Pd^{III} complex as compared to Pd^{II} complex. Similar studies were conducted with iodobenzene as a model substrate, which showed similar results within 1 h to indicate faster coupling reactions with aryl iodides as compared to aryl chlorides

(Fig. 12-(b)).

To gain further insight into the reaction mechanism, several controlled experiments were carried out (Scheme 4). The mercury drop experiment was carried out to assess the homogeneous nature of the catalysis. Addition of a drop of mercury to the catalytic reaction did not affect the reaction and yield of the product, thus confirming the homogeneous nature of the coupling reaction. In order to rule out the possibility of radical pathway, separate reactions were performed using the optimized conditions in the presence of a radical scavenger such as hydroquinone and radical initiator such as di-*tert*-butylperoxide. In both cases yield remained unaffected, proving the absence of a radical mechanism. A gram scale reaction conducted under optimal reaction conditions resulted in an impressive 96 % yield.

4. Conclusions

A new amide based PN(H)N ligand was synthesised and its Pd and Pt metal chemistry has been explored. Suzuki-Miyaura cross coupling reaction between aryl halides and boronic acids was studied in detail using Pd complex 4, which was found to proceed through Pd^{II}/Pd^{III}/Pd^{IV} catalytic cycle. The Pd^{III} species was detected using mass spectrometry, NMR, XPS and EPR techniques. Detailed mechanistic study using DFT calculations (B3LYP-D3/def2-TZVP) revealed the involvement of various oxidation states of palladium in the cross-coupling reaction. The computed results revealed that the Pd^{III} complex is short-lived and converts rapidly into Pd^{IV} complex. Mass spectrometry and XPS plot also confirmed the presence of Pd^{IV} species. Further, CV studies were conducted to highlight the importance of base in the reaction. Additionally, this investigation encompasses comparative rate studies that contrast aryl iodides and aryl chlorides in Suzuki coupling reaction. These studies yield valuable insight into the reaction kinetics and substrate specificity, enhancing our understanding of the process. The catalytic process with a very low catalyst loading performed well under moderate reaction conditions. Similar pincer complexes of nickel, manganese and

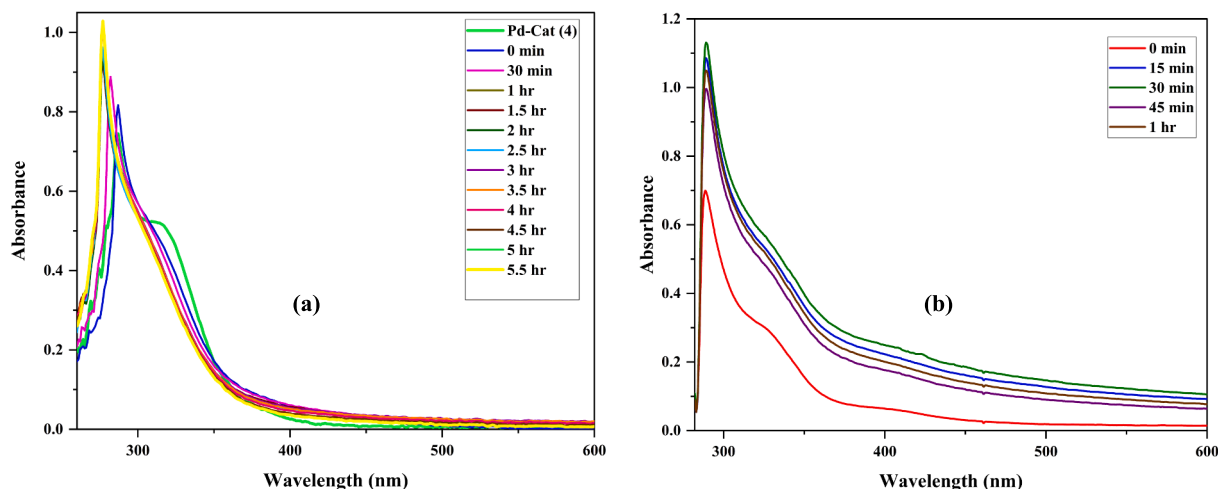
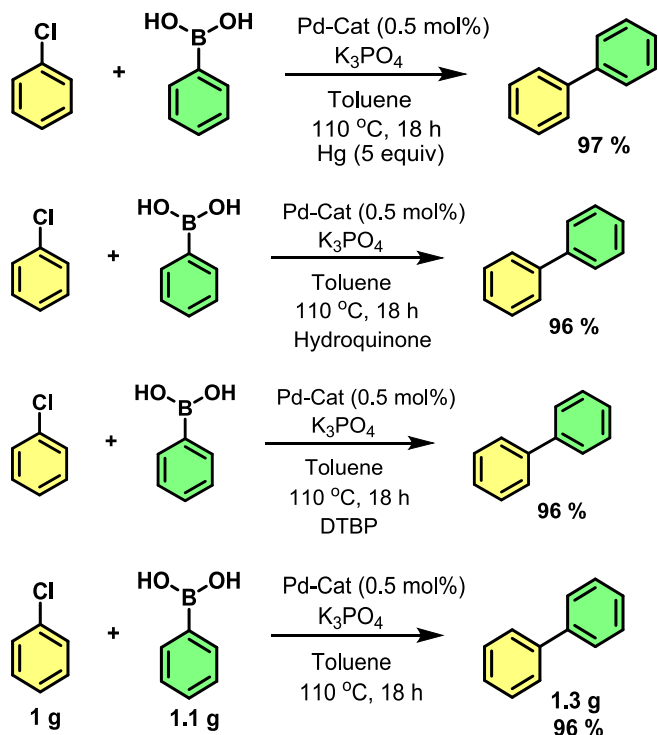


Fig. 12. UV plots for Suzuki-Miyaura Coupling reaction monitored at 90 °C for 5.5 h in case of chlorobenzene as a reactant (a) and monitored at 90 °C for 1 h in case of iodobenzene as a reactant (b).



Scheme 4. Controlled experiments and mechanistic investigation.

ruthenium have the potential to catalyse many organic transformations. The work in this direction is under active investigation in our laboratory.

Author contributions

The manuscript was written through contributions of all authors. All authors have given approval to the final version of the manuscript.

CRediT authorship contribution statement

Gazal Sabharwal: Writing – original draft, Conceptualization. **Khilesh C. Dwivedi:** Investigation. **Chandan Das:** Investigation, Formal analysis. **Thakur Rochak Kumar Rana:** Writing – original draft, Software, Formal analysis. **Arnab Dutta:** Writing – original draft, Formal analysis. **Gopalan Rajaraman:** Software, Formal analysis, Data

curation. **Maravanji S. Balakrishna:** Writing – review & editing, Supervision, Methodology, Conceptualization.

Declaration of competing interest

The authors declare that they have no known competing financial interests or personal relationships that could have appeared to influence the work reported in this paper.

Acknowledgments

MSB thank Indian Institute of Technology Bombay for supporting this work through Research Development Fund (RDF). We are thankful to the Department of Chemistry, IIT Bombay, for instrumentation facilities, as well as spectral and analytical data. GS and CD thank IITB for fellowships, KCD thanks UGC, New Delhi for JRF/SRF fellowships, TRKR acknowledges the financial support from the Prime Minister's Research Fellowship (PMRF).

Appendix A. Supplementary data

Spectroscopic results, as well as computational details (PDF). Computational structures (XYZ). Crystallographic information (CIF). Supplementary data to this article can be found online at <https://doi.org/10.1016/j.jcat.2024.115825>.

Data availability

Data will be made available on request.

References

- [1] H. Guo, Y.C. Fan, Z. Sun, Y. Wu, O. Kwon, Phosphine organocatalysis, *Chem. Rev.* 118 (2018) 10049–10293.
- [2] D.W. Allen, Phosphines and related C–P bonded compounds, in: D.W. Allen, D. Loakes, J.C. Tebby (Eds.), *Organophosphorus Chemistry*, The Royal Society of Chemistry, 2016, pp. 0.
- [3] C. Müller, D. Vogt, Phosphinines as ligands in homogeneous catalysis: recent developments, concepts and perspectives, *Dalton Trans.* 5505–5523 (2007).
- [4] M.J. Buskes, M.-J. Blanco, Impact of cross-coupling reactions in drug discovery and development, *Mol.* 25 (2020) 3493.
- [5] S. Sheokand, M.S. Balakrishna, Cationic and neutral Pd^{II} and Pt^{II} Pincer complexes of phosphinamino-triazolyl-pyridine [PN(H)N]: pincer ligand-stabilized palladium nanoparticles and their catalytic annulation of internal alkynes to indenones, *Inorg. Chem.* 62 (2023) 12317–12328.
- [6] P.K. Namdeo, S. Sheokand, B.S. Kote, L. Radhakrishna, H.S. Kunchur, P. Saini, S. Ramakrishnan, M.S. Balakrishna, Ru^{II} complexes of 1,2,3-triazole appended tertiary phosphines, [P(Ph){(o-C₆H₄)(1,2,3-N₃C(Ph)CH₂)₂} and [P(Ph){o-

- C₆H₄(CCH-(1,2,3-N₃-Ph))₂: highly active catalysts for transfer hydrogenation of carbonyl/nitro compounds and for α -alkylation of ketones, *Dalton Trans.* 51 (2022) 6795–6808.
- [7] V.S. Kashid, L. Radhakrishna, M.S. Balakrishna, First examples of tri- and tetraphosphametacyclophanes: synthesis and isolation of an unusual hexapalladium complex containing pincer units with Pd–P covalent bonds, *Dalton Trans.* 46 (2017) 6510–6513.
- [8] G. Neitzel, R. Razaq, A. Spannenberg, K. Stier, M.P. Checinski, R. Jackstell, M. Beller, An improved manganese pincer catalyst for low temperature hydrogenation of carbon monoxide to methanol, *ChemCatChem* 16 (2024) e202301053.
- [9] G.S. Ananthnag, D. Mondal, J.T. Mague, M.S. Balakrishna, Synthesis of tetra-pincer nickel(II) and palladium(III) complexes of resorcin[4]arene-octaphosphinite [Res (OPR₂)₈] and rhodium-catalyzed regioselective hydroformylation reaction, *Dalton Trans.* 48 (2019) 14632–14641.
- [10] E. Peris, R.H. Crabtree, Key factors in pincer ligand design, *Chem. Soc. Rev.* 47 (2018) 1959–1968.
- [11] L. Piccirilli, D. Lobo Justo Pinheiro, M. Nielsen, Recent progress with pincer transition metal catalysts for sustainability, *Catal.* 10 (2020) 773.
- [12] X.-F. Wu, P. Anbarasan, H. Neumann, M. Beller, From noble metal to nobel prize: palladium-catalyzed coupling reactions as key methods in organic synthesis, *Angew. Chem. Int. Ed.* 49 (2010) 9047–9050.
- [13] L. Xue, Z. Lin, Theoretical aspects of palladium-catalyzed carbon–carbon cross-coupling reactions, *Chem. Soc. Rev.* 39 (2010) 1692–1705.
- [14] P. Gautam, N.J. Tiwari, B.M. Bhanage, Aminophosphine palladium pincer-catalyzed carbonylative sonogashira and suzuki-miyaura cross-coupling with high catalytic turnovers, *ACS Omega* 4 (2019) 1560–1574.
- [15] A. Maji, A. Singh, A. Mohanty, P.K. Maji, K. Ghosh, Ferrocenyl palladacycles derived from unsymmetrical pincer-type ligands: evidence of Pd(0) nanoparticle generation during the Suzuki-Miyaura reaction and applications in the direct arylation of thiazoles and isoxazoles, *Dalton Trans.* 48 (2019) 17083–17096.
- [16] M.C. D'Alterio, E. Casals-Cruañas, N.V. Tzouras, G. Talarico, S.P. Nolan, A. Poater, Mechanistic aspects of the palladium-catalyzed Suzuki-Miyaura cross-coupling reaction, *Chem. Eur. J.* 27 (2021) 13481–13493.
- [17] O. Blacque, C.M. Frech, Pincer-type heck catalysts and mechanisms based on Pd^{IV} intermediates: a computational study, *Chem. Eur. J.* 16 (2010) 1521–1531.
- [18] K. Muñiz, High-oxidation-state palladium catalysis: new reactivity for organic synthesis, *Angew. Chem. Int. Ed.* 48 (2009) 9412–9423.
- [19] A.J. Hickman, M.S. Sanford, High-valent organometallic copper and palladium in catalysis, *Nat.* 484 (2012) 177–185.
- [20] L.K. Burt, C.C. Ho, High oxidation state organopalladium(IV) species: applications to C–H activation, *Aust. J. Chem.* 71 (2018) 753–755.
- [21] G. Yin, X. Mu, G. Liu, Palladium(II)-catalyzed oxidative difunctionalization of alkenes: bond forming at a high-valent palladium center, *Acc. Chem. Res.* 49 (2016) 2413–2423.
- [22] D. Milstein, J.K. Stille, Mechanism of reductive elimination. reaction of alkylpalladium(II) complexes with tetraorganotin, organolithium, and Grignard reagents. Evidence for palladium(IV) intermediacy, *J. Am. Chem. Soc.* 101 (1979) 4981–4991.
- [23] A. Sundermann, O. Uzan, J.M.L. Martin, Computational study of a new heck reaction mechanism catalyzed by palladium(II/IV) species, *Chem. Eur. J.* 7 (2001) 1703–1711.
- [24] D.C. Powers, T. Ritter, Bimetallic Pd(III) complexes in palladium-catalyzed carbon–heteroatom bond formation, *Nat. Chem.* 1 (2009) 302–309.
- [25] S. Panja, S. Ahsan, T. Pal, S. Kolb, W. Ali, S. Sharma, C. Das, J. Grover, A. Dutta, D. B. Werz, A. Paul, D. Maiti, Non-directed Pd-catalyzed electrooxidative olefination of arenes, *Chem. Sci.* 13 (2022) 9432–9439.
- [26] J.M. Racowski, N.D. Ball, M.S. Sanford, C–H bond activation at palladium(IV) centers, *J. Am. Chem. Soc.* 133 (2011) 18022–18025.
- [27] F. Visentin, C. Santo, T. Scattolin, N. Demitri, L. Canovese, Reactivity of N-heterocyclic carbene–pyridine palladacyclopentadiene complexes toward halogen addition. The Unpredictable Course of the Reaction, *Dalton Trans.* 46 (2017) 10399–10407.
- [28] J.R. Brandt, E. Lee, G.B. Boursalian, T. Ritter, Mechanism of electrophilic fluorination with Pd(IV): fluoride capture and subsequent oxidative fluoride transfer, *Chem. Sci.* 5 (2014) 169–179.
- [29] F. Tang, Y. Zhang, N.P. Rath, L.M. Mirica, Detection of Pd(III) and Pd(IV) intermediates during the aerobic oxidative C–C bond formation from a Pd(II) dimethyl complex, *Organometallics* 31 (2012) 6690–6696.
- [30] J. Vicente, A. Arcas, F. Juliá-Hernández, D. Bautista, Synthesis of a Palladium(IV) complex by oxidative addition of an aryl halide to palladium(II) and its use as precatalyst in a C–C coupling reaction, *Angew. Chem. Int. Ed.* 50 (2011) 6896–6899.
- [31] F. Qu, J.R. Khusnutdinova, N.P. Rath, L.M. Mirica, Dioxxygen activation by an organometallic Pd(II) precursor: formation of a Pd(IV)–OH complex and its C–O bond formation reactivity, *Chem. Commun.* 50 (2014) 3036–3039.
- [32] B. Zhang, X. Yan, S. Guo, Synthesis of well-defined high-valent palladium complexes by oxidation of their palladium(II) precursors, *Chem. Eur. J.* 26 (2020) 9430–9444.
- [33] P.K. Byers, A.J. Canty, B.W. Skelton, A.H. White, The oxidative addition of iodomethane to [PdMe₂(bpy)] and the X-ray structure of the organopalladium(IV) product fac-[PdMe₃(bpy)](bpy = 2,2'-bipyridyl), *J. Chem. Soc., Chem. Commun.* (1986) 1722–1724.
- [34] A. Maleckis, M.S. Sanford, Facial tridentate ligands for stabilizing palladium(IV) complexes, *Organometallics* 30 (2011) 6617–6627.
- [35] N.P. Ruhs, J.R. Khusnutdinova, N.P. Rath, L.M. Mirica, Mononuclear organometallic Pd(II), Pd(III), and Pd(IV) complexes stabilized by a pyridinophane ligand with a C-donor group, *Organometallics* 38 (2019) 3834–3843.
- [36] D.C. Powers, E. Lee, A. Ariafard, M.S. Sanford, B.F. Yates, A.J. Canty, T. Ritter, Connecting binuclear Pd(III) and mononuclear Pd(IV) chemistry by Pd–Pd bond cleavage, *J. Am. Chem. Soc.* 134 (2012) 12002–12009.
- [37] F. Tang, F. Qu, J.R. Khusnutdinova, N.P. Rath, L.M. Mirica, Structural and reactivity comparison of analogous organometallic Pd(III) and Pd(IV) complexes, *Dalton Trans.* 41 (2012) 14046–14050.
- [38] L.-M. Xu, B.-J. Li, Z. Yang, Z.-J. Shi, Organopalladium(IV) chemistry, *Chem. Soc. Rev.* 39 (2010) 712–733.
- [39] S.H. Eitel, M. Bauer, D. Schweinfurth, N. Deibel, B. Sarkar, H. Kelm, H.-J. Krüger, W. Frey, R. Peters, Paramagnetic palladacycles with Pd^{III} centers are highly active catalysts for asymmetric aza-claisen rearrangements, *J. Am. Chem. Soc.* 134 (2012) 4683–4693.
- [40] F.A. Cotton, I.O. Koshevoy, P. Lahuerta, C.A. Murillo, M. Sanaú, M.A. Ubeda, Q. Zhao, High yield syntheses of stable, singly bonded Pd³⁺ compounds, *J. Am. Chem. Soc.* 128 (2006) 13674–13675.
- [41] M. Sharma, A. Ariafard, A.J. Canty, M.G. Gardiner, R.C. Jones, Synthetic and computational studies of the palladium(IV) system Pd(alkyl)(aryl)(alkynyl) (bidentate)(triflate) exhibiting selectivity in C–C reductive elimination, *Dalton Trans.* 41 (2012) 11820–11828.
- [42] K.J. Bonney, F. Schoenebeck, Experiment and computation: a combined approach to study the reactivity of palladium complexes in oxidation states 0 to IV, *Chem. Soc. Rev.* 43 (2014) 6609–6638.
- [43] P. Veerakumar, P. Thanasekaran, K.-L. Lu, K.-C. Lin, S. Rajagopal, Computational studies of versatile heterogeneous palladium-catalyzed Suzuki, Heck, and Sonogashira coupling reactions, *ACS Sustainable Chem. Eng.* 5 (2017) 8475–8490.
- [44] K.W. Quasdorf, A. Antoft-Finch, P. Liu, A.L. Silberstein, A. Komaromi, T. Blackburn, S.D. Ramgren, K.N. Houk, V. Snieckus, N.K. Garg, Suzuki–Miyaura cross-coupling of aryl carbamates and sulfamates: experimental and computational studies, *J. Am. Chem. Soc.* 133 (2011) 6352–6363.
- [45] A.A.C. Braga, N.H. Morgon, G. Ujaque, A. Lledós, F. Maseras, Computational study of the transmetalation process in the Suzuki-Miyaura cross-coupling of aryls, *J. Organomet. Chem.* 691 (2006) 4459–4466.
- [46] D. Drew, J.R. Doyle, A.G. Shaver, Cyclic Diolenin complexes of platinum and palladium, *Inorg. Synth.* (1990) 346–349.
- [47] O.V. Dolomanov, L.J. Bourhis, R.J. Gildea, J.A.K. Howard, H. Puschmann, OLEX2: a complete structure solution, refinement and analysis program, *J. Appl. Crystallogr.* 42 (2009) 339–341.
- [48] G. Sheldrick, SHELXT - Integrated space-group and crystal-structure determination, *Acta Crystallogr.* 71 (2015) 3–8.
- [49] G. Sheldrick, Crystal structure refinement with SHELXL, *Acta Crystallogr.* 71 (2015) 3–8.
- [50] A.D. Becke, Density-functional thermochemistry. V. Systematic optimization of exchange-correlation functionals, *J. Chem. Phys.* 107 (1997) 8554–8560.
- [51] J. Antony, S. Grimme, Density functional theory including dispersion corrections for intermolecular interactions in a large benchmark set of biologically relevant molecules, *Phys. Chem. Chem. Phys.* 8 (2006) 5287–5293.
- [52] L.E. Roy, P.J. Hay, R.L. Martin, Revised basis sets for the LANL effective core potentials, *J. Chem. Theory Comput.* 4 (2008) 1029–1031.
- [53] A.V. Mitin, J. Baker, P. Pulay, An improved 6–31G* basis set for first-row transition metals, *J. Chem. Phys.* 118 (2003) 7775–7782.
- [54] A.D. Becke, Density-functional exchange-energy approximation with correct asymptotic behavior, *Phys. Rev. A* 38 (1988) 3098–3100.
- [55] M.R. Silva-Junior, M. Schreiber, S.P.A. Sauer, W. Thiel, Benchmarks of electronically excited states: basis set effects on CASPT2 results, *J. Chem. Phys.* 133 (2010).
- [56] J. Tomasi, B. Mennucci, R. Cammi, Quantum mechanical continuum solvation models, *Chem. Rev.* 105 (2005) 2999–3094.
- [57] E.D. Glendening, C.R. Landis, F. Weinhold, NBO 6.0: natural bond orbital analysis program, *J. Comput. Chem.* 34 (2013) 1429–1437.
- [58] T.R.K. Rana, A. Swain, G. Rajaraman, The role of agostic interaction in the mechanism of ethylene polymerisation using Cr(III) half-sandwich complexes: What dictates the reactivity? *Dalton Trans.* 52 (2023) 11826–11834.
- [59] I. Mayer, Bond orders and valences in the SCF theory: a comment, *Theor. Chim. Acta* 67 (1985) 315–322.
- [60] Y. Guo, C. Riplinger, U. Becker, D.G. Liakos, Y. Minenkov, L. Cavallo, F. Neese, Communication: an improved linear scaling perturbative triples correction for the domain based local pair-natural orbital based singles and doubles coupled cluster method [DLPNO-CCSD(T)], *J. Chem. Phys.* 148 (2018).
- [61] S.E. Neale, D.A. Pantazis, S.A. Macgregor, Accurate computed spin-state energetics for Co(III) complexes: implications for modelling homogeneous catalysis, *Dalton Trans.* 49 (2020) 6478–6487.
- [62] F. Neese, Software update: The ORCA program system—Version 5.0, *Wiley Interdiscip. Rev. Comput. Mol. Sci.* 12 (2022) e1606.
- [63] P. Paiva, M.J. Ramos, P.A. Fernandes, Assessing the validity of DLPNO-CCSD(T) in the calculation of activation and reaction energies of ubiquitous enzymatic reactions, *J. Comput. Chem.* 41 (2020) 2459–2468.
- [64] M.E. Broussard, B. Juma, S.G. Train, W.-J. Peng, S.A. Laneman, G.G. Stanley, A bimetallic hydroformylation catalyst: high regioselectivity and reactivity through homobimetallic cooperativity, *Science* 260 (1993) 1784–1788.
- [65] M. Douglas, N.M. Kroll, Quantum electrodynamic corrections to the fine structure of helium, *Ann. Phys.* 82 (1974) 89–155.
- [66] M.K. Pandey, H.S. Kunchur, D. Mondal, L. Radhakrishna, B.S. Kote, M. S. Balakrishna, Rare Au–H interactions in Gold(I) complexes of bulky phosphines

- derived from 2,6-dibenzhydryl-4-methylphenyl core, *Inorg. Chem.* 59 (2020) 3642–3658.
- [67] S. Kumar, J. Jyoti, D. Gupta, G. Singh, A. Kumar, A decade of exploration of transition-metal-catalyzed cross-coupling reactions: an overview, *SynOpen* 7 (2023) 580–614.
- [68] A. Ahmed, I. Mushtaq, S. Chinnam, Suzuki-Miyaura cross-couplings for alkyl boron reagent: recent developments—a review, *Future J. Pharm. Sci.* 9 (2023) 67.
- [69] B.S. Kadu, Suzuki-Miyaura cross coupling reaction: recent advancements in catalysis and organic synthesis, *Catal. Sci. Technol.* 11 (2021) 1186–1221.
- [70] S. Kotha, K. Lahiri, D. Kashinath, Recent applications of the Suzuki-Miyaura cross-coupling reaction in organic synthesis, *Tetrahedron* 58 (2002) 9633–9695.
- [71] L. González-Sebastián, D. Morales-Morales, Cross-coupling reactions catalysed by palladium pincer complexes. A review of recent advances, *J. Organomet. Chem.* 893 (2019) 39–51.
- [72] L. Hettmanczyk, B. Schmid, S. Hohloch, B. Sarkar, Palladium(II)-acetylacetonato complexes with mesoionic carbenes: synthesis, structures and their application in the Suzuki-Miyaura cross coupling reaction, *Mol.* 21 (2016) 1561.
- [73] R. Maity, A. Verma, M. van der Meer, S. Hohloch, B. Sarkar, Palladium complexes bearing mesoionic carbene ligands: applications in α -arylation, α -methylation and Suzuki-Miyaura coupling reactions, *Eur. J. Inorg. Chem.* 2016 (2016) 111–117.
- [74] Z. Cao, Q. Wang, H. Neumann, M. Beller, Regiodivergent carbonylation of alkenes: selective palladium-catalyzed synthesis of linear and branched selenoesters, *Angew. Chem. Int. Ed.* 63 (2024) e202313714.
- [75] Á. Molnár, Palladium-catalyzed coupling reactions: practical aspects and future developments, John Wiley & Sons, 2013.
- [76] Yin, J. Liebscher, Carbon-carbon coupling reactions catalyzed by heterogeneous palladium catalysts, *Chem. Rev.* 107 (2007) 133–173.
- [77] A. Biffis, P. Centomo, A. Del Zotto, M. Zecca, Pd metal catalysts for cross-couplings and related reactions in the 21st century: a critical review, *Chem. Rev.* 118 (2018) 2249–2295.
- [78] A.F. Littke, G.C. Fu, Palladium-catalyzed coupling reactions of aryl chlorides, *Angew. Chem. Int. Ed.* 41 (2002) 4176–4211.
- [79] P. Orecchia, D.S. Petkova, R. Goetz, F. Rominger, A.S.K. Hashmi, T. Schaub, Pd-Catalysed Suzuki-Miyaura cross-coupling of aryl chlorides at low catalyst loadings in water for the synthesis of industrially important fungicides, *Green Chem.* 23 (2021) 8169–8180.
- [80] R. Martin, S.L. Buchwald, Palladium-catalyzed Suzuki-Miyaura cross-coupling reactions employing dialkylbiaryl phosphine ligands, *Acc. Chem. Res.* 41 (2008) 1461–1473.
- [81] M.J. Frisch, G.W. Trucks, H.B. Schlegel, G.E. Scuseria, M.A. Robb, J.R. Cheeseman, G. Scalmani, V. Barone, G.A. Petersson, H. Nakatsuji, X. Li, M. Caricato, A.V. Marenich, J. Bloino, B.G. Janesko, R. Gomperts, B. Mennucci, H.P. Hratchian, J.V. Ortiz, A.F. Izmaylov, J.L. Sonnenberg, Williams, F. Ding, F. Lipparini, F. Egidi, J. Goings, B. Peng, A. Petrone, T. Henderson, D. Ranasinghe, V.G. Zakrzewski, J. Gao, N. Rega, G. Zheng, W. Liang, M. Hada, M. Ehara, K. Toyota, R. Fukuda, J. Hasegawa, M. Ishida, T. Nakajima, Y. Honda, O. Kitao, H. Nakai, T. Vreven, K. Throssell, J.A. Montgomery Jr., J.E. Peralta, F. Ogliaro, M.J. Bearpark, J.J. Heyd, E.N. Brothers, K.N. Kudin, V.N. Staroverov, T.A. Keith, R. Kobayashi, J. Normand, K. Raghavachari, A.P. Rendell, J.C. Burant, S.S. Iyengar, J. Tomasi, M. Cossi, J.M. Millam, M. Klene, C. Adamo, R. Cammi, J.W. Ochterski, R.L. Martin, K. Morokuma, O. Farkas, J.B. Foresman, D.J. Fox, *Gaussian 16 Rev. C.01*, Wallingford, CT, 2016.
- [82] A.A.C. Braga, N.H. Morgon, G. Ujaque, F. Maseras, Computational characterization of the role of the base in the Suzuki-Miyaura cross-coupling reaction, *J. Am. Chem. Soc.* 127 (2005) 9298–9307.
- [83] A.A. Thomas, A.F. Zahrt, C.P. Delaney, S.E. Denmark, Elucidating the role of the boronic esters in the Suzuki-Miyaura Reaction: structural, kinetic, and computational investigations, *J. Am. Chem. Soc.* 140 (2018) 4401–4416.
- [84] L.L. Liu, S. Zhang, H. Chen, Y. Lv, J. Zhu, Y. Zhao, Mechanistic insight into the nickel-catalyzed cross-coupling of aryl phosphates with arylboronic acids: potassium phosphate is not a spectator base but is involved in the transmetalation step in the Suzuki-Miyaura reaction, *Chem. Asian J.* 8 (2013) 2592–2595.
- [85] A.A.C. Braga, G. Ujaque, F. Maseras, A DFT study of the full catalytic cycle of the Suzuki-Miyaura cross-coupling on a model system, *Organometallics* 25 (2006) 3647–3658.
- [86] M. García-Melchor, A.A.C. Braga, A. Lledós, G. Ujaque, F. Maseras, Computational perspective on Pd-catalyzed C-C cross-coupling reaction mechanisms, *acc. Chem. Res.* 46 (2013) 2626–2634.
- [87] Z.-Y. Xu, H.-Z. Yu, Y. Fu, Mechanism of nickel-catalyzed Suzuki-Miyaura coupling of amides, *Chem. Asian J.* 12 (2017) 1765–1772.
- [88] T. Mondal, S. De, S. Dutta, D. Koley, Mechanistic exploration of the transmetalation and reductive elimination events involving PdIV-abnormal NHC complexes in Suzuki-Miyaura coupling reactions: a DFT study, *Chem. Eur. J.* 24 (2018) 6155–6168.
- [89] M. Pareek, R.B. Sunoj, Energetics of dynamic kinetic asymmetric transformation in Suzuki-Miyaura coupling, *ACS Catal.* 10 (2020) 4349–4360.
- [90] S. Kozuch, J.M.L. Martin, What makes for a bad catalytic cycle? A theoretical study on the Suzuki-Miyaura reaction within the energetic span model, *ACS Catal.* 1 (2011) 246–253.
- [91] L.L. Liu, P. Chen, Y. Sun, Y. Wu, S. Chen, J. Zhu, Y. Zhao, Mechanism of nickel-catalyzed selective C-N bond activation in Suzuki-Miyaura cross-coupling of amides: a theoretical investigation, *J. Org. Chem.* 81 (2016) 11686–11696.
- [92] J.R. Khushnutdinova, N.P. Rath, L.M. Mirica, Stable mononuclear organometallic Pd(III) complexes and their C-C bond formation reactivity, *J. Am. Chem. Soc.* 132 (2010) 7303–7305.
- [93] S.K. Singh, M. Atanasov, F. Neese, Challenges in multireference perturbation theory for the calculations of the g-tensor of first-row transition-metal complexes, *J. Chem. Theory Comput.* 14 (2018) 4662–4677.